Inorganic Chemistry
Article

Inorg. Chem. **2011**, *50*, 647–655 **647**
DOI: 10.1021/ic101846f

Perovskite-Type Metal Oxides Exhibiting Negligible Grain Boundary Resistance to Total Electrical Conductivity

Tania Pannu, Kanwar Gulsher Singh Pannu, and Venkataraman Thangadurai*

Department of Calgary, University of Calgary, 2500 University Drive Northwest, Calgary, AB T2N 1N4, Canada

Received September 8, 2010

In this paper, we report the synthesis, structure and electrical properties of the perovskite-type $AZn_{0.33+x}Nb_{0.67-x}O_{3-\delta}$ (A = Sr or Ba; $0 \leq x \leq 0.08$). The investigated compounds were prepared by employing the solid-state (ceramic) reaction using alkaline nitrates, zinc oxide, and niobium oxide at elevated temperatures in air. Powder X-ray diffraction (PXRD) showed the formation of disordered Zn and Nb at the B-sites of space group $Pm\bar{3}m$ with cubic structure and a lattice constant comparable to that of the literature. The AC impedance study showed mainly bulk contribution to the total electrical conductivity over the investigated frequency range of 0.01 Hz to 1 MHz in all the investigated atmospheres even at low temperatures, which is significantly different from that of the well-known perovskite-type B-site ordered $BaCa_{0.33+x}Nb_{0.67-x}O_{3-\delta}$ and the disordered acceptor-doped $BaCeO_3$. The bulk dielectric constant determined at 500 and 700 °C in air was found to be in the range of 35−100. In air, the isothermal bulk dielectric constant seems to increase with an increasing Zn content, and a similar trend was observed for total electrical conductivity. In dry and wet H_2, the electrical conductivity decreases with an increasing Zn content in $AZn_{0.33+x}Nb_{0.67-x}O_{3-\delta}$, and the $x = 0$ member of the Ba compound exhibits the highest total conductivity of 7.2×10^{-3} S cm^{-1} in dry H_2 at 800 °C. Both Sr and Ba compounds were found to be stable against the reaction with pure CO_2 at 700 °C and H_2O at 100 °C for a long period of time. $SrZn_{0.33+x}Nb_{0.67-x}O_{3-\delta}$ was found to be stable in 30 ppm H_2S at 800 °C, while the corresponding Ba compound formed reaction products such as BaS (JCPDS Card 01-0757), BaS_2 (JCPDS Card 21-0087), and BaS_3 (JCPDS Card 03-0824).

1. Introduction

Current research on solid oxide fuel cells (SOFCs) has gained extensive popularity in the field of electrical energy production because of their high electrical efficiency in the conversion from chemical energy to electrical energy, cleanliness, and fuel flexibility such as H_2, alcohols, alkanes, and NH_3. On the basis of the membrane, SOFCs can further be classified into two types, namely, oxide ion-conducting SOFCs (O-SOFCs) and proton-conducting SOFCs (H-SOFCs). The development of the former type of SOFCs is based on the conventional fluorite-type Y_2O_3-doped ZrO_2 (YSZ) electrolyte, perovskite-like Sr-doped $LaMnO_3$ (LSM) cathode, and Ni-YSZ composite anode.[1−6] However, the Ni-YSZ anode is very unstable in C- and S-containing atmospheres, and LSM reacts with the YSZ electrolyte at elevated temperatures, forming electronically insulating and poorly ionic conducting reaction products (e.g., $SrZrO_3$ and $La_2Zr_2O_7$), thus limiting its lifetime and decreasing the overall performance.[7−9] This problem seems primarily due to the requirement of a high operating temperature of 800−1000 °C to allow appreciable ionic conduction in YSZ. Attempts have been made to replace various oxide ion electrolytes in the O-SOFCs to overcome the long-term chemical stability issues.

The latter approach involves the replacement of the oxide ion electrolytes with proton conductors to overcome the materials problem of the O-SOFCs. Furthermore, unlike O-SOFCs, the reaction product will be formed at the cathode side in the case of H-SOFCs. Various electrolyte materials of H-SOFCs have been investigated after Iawahra's discovery of the fast proton conduction in acceptor-doped perovskites in humidified atmospheres.[10] For example, Y_2O_3-doped $BaCeO_3$ (BCY) is being considered as a membrane for H-SOFCs, which exhibits good proton conductivity in wet H_2 at elevated temperatures. However, there are several problems with BCY such as its poor chemical stability in CO_2 atmospheres

*To whom correspondence should be addressed. E-mail: vthangad@ucalgary.ca. Phone: (403) 210-8649. Fax: (403) 210-9364.

(1) Sun, C.; Stimming, U. *J. Power Sources* **2007**, *171*, 247–260.
(2) Atkinson, A.; Barnett, S.; Gorte, R. J.; Irvine, J. T. S.; Mcevoy, A. J.; Mogensen, M.; Singhal, S. C.; Vohs, J. *Nat. Mater.* **2004**, *3*, 17–27.
(3) Brandon, N. P.; Skinner, S.; Steele, B. C. H. *Annu. Rev. Mater. Res.* **2003**, *33*, 183–213.
(4) Carrette, L.; Friedrich, K. A.; Stimming, U. *Fuel Cells* **2001**, *1*, 5–39.
(5) Wincewicz, K.; Cooper, J. S. *J. Power Sources* **2005**, *140*, 280–296.
(6) Tao, S.; Irvine, J. T. S. *Chem. Rec.* **2004**, *4*, 83–95.
(7) Miao, H.; Wang, W. G.; Li, T. S.; Chen, T.; Sun, S. S.; Xu, C. *J. Power Sources* **2010**, *195*, 2230–2235.
(8) Cheng, Z.; Liu, M. *Solid State Ionics* **2007**, *178*, 925–935.
(9) Fergus, J. W. *Solid State Ionics* **2006**, *177*, 1529–1541.
(10) Iwahara, H.; Esaka, T.; Uchida, H.; Yamauchi, T.; Ogaki, K. *Solid State Ionics* **1986**, *18−19*, 1003–1007.

© 2010 American Chemical Society
Published on Web 12/09/2010

and at high levels of humidity. Attempts have been made to improve the chemical stability and to maintain high proton conductivity, simultaneously. Partial replacement of Ce with Zr in BCY was found to improve the chemical stability in CO_2,[11−18] but the proton conductivity decreases with the increasing Zr content and shows large grain boundary resistance.[11,12] Solid acids, organic polymers, and metal oxide hydrate-based materials exhibit low-temperature stability, and their conductivity depends on humidity.

Nowick and Du discovered ordered perovskite-type $BaCa_{0.33+x}Nb_{0.67-x}O_{3-\delta}$ (BCN),[19] which not only shows good bulk conductivity but also shows chemical stability in various media, making it suitable to be considered as an electrolyte for H-SOFCs.[20−22] However, the major challenge with BCN ceramics is the excessively large grain boundary resistance and poor electrode−electrolyte interface connection, thus decreasing the overall performance of the fuel cell. Recently, Tao and Irvine proposed to substitute Zn in the perovskite BCY, which not only decreased the sintering temperature, but also improved the density and hence the total (bulk + grain boundary) electrical conductivity.[16,23]

Here, for the first time, we report the chemical stability and electrical transport properties of the nonstoichiometric Zn-based perovskite-type $AZn_{0.33+x}Nb_{0.67-x}O_{3-\delta}$ (A = Sr or Ba; $0 \le x \le 0.08$) in various atmospheres, including ambient air, wet N_2, dry H_2, and wet H_2. Our results show that unlike the well-known BCN, the investigated compounds exhibited mainly bulk contribution to the total conductivity, and moreover, the conductivity was found to increase in the D_2O-containing atmosphere compared to the H_2O medium. Among the samples investigated, $BaZn_{0.33}Nb_{0.67}O_3$ exhibited the highest total conductivity of 7.2×10^{-3} S cm^{-1} in dry H_2 at 800 °C.

2. Experimental Aspects

Preparation of Perovskite-Type $AZn_{0.33+x}Nb_{0.67-x}O_{3-\delta}$ (A = Sr or Ba; $0 \le x \le 0.08$). Metal oxides with nominal chemical formulas of $SrZn_{0.33+x}Nb_{0.67-x}O_{3-\delta}$ (SZN) and $BaZn_{0.33+x}Nb_{0.67-x}O_{3-\delta}$ (BZN) were synthesized using the ceramic method using appropriate amounts of high-purity $Sr(NO_3)_2$ (99.0%, Alfa Aesar), $Ba(NO_3)_2$ (99.0%, Alfa Aesar), Nb_2O_5 (99.5%, Alfa Aesar), and ZnO (99.0%, Alfa Aesar). The powders were mixed using a ball mill (Pulverisette, Fritsch, Germany) at 200 rpm for 6 h using zirconia balls and 2-propanol with an intermediate change in the rotation direction every 1 h to ensure proper mixing. The resultant mixture was then dried and calcinated at 900 °C for 12 h in air in a clean alumina crucible. The resulting mixture was ball-milled again with 2-propanol for 6 h at 200 rpm, after which the powders were pressed into pellets (~1 cm diameter and ~2 cm length) using an isotatic pressure. The pellets were then sintered in air at 1450 °C for the Sr compound and 1400 °C for the Ba compound for 12 h at a ramp rate of 5 °C/min. The sintered powders were then crushed using a mortar and pestle until they were fine for the powder X-ray diffraction analysis (PXRD) using a Bruker D8 powder X-ray diffractometer (40 kV, 40 mA, Cu Kα) with a 2θ step scan width of 0.02° and a counting time of 6 s.

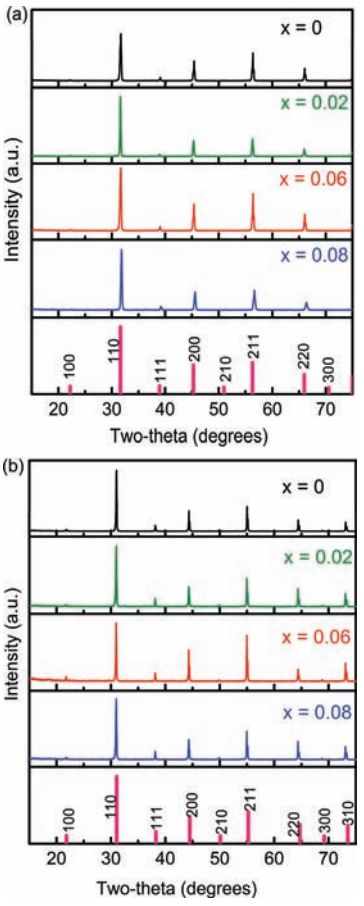

Figure 1. Powder XRD patterns of (a) $SrZn_{0.33+x}Nb_{0.67-x}O_{3-\delta}$ and (b) $BaZn_{0.33+x}Nb_{0.67-x}O_{3-\delta}$ ($x = 0$, 0.02, 0.06, or 0.08). For comparison, we show the simple cubic perovskite-type $x = 0$ member reported in the literature[24b] in the bottom of the panel. The Miller indices (*hkl*) of the XRD peaks are shown for the parent ($x = 0$) compound.[24]

Investigation of the Chemical Stability. The synthesized compounds ($AZn_{0.33+x}Nb_{0.67-x}O_{3-\delta}$) were tested for their chemical stability in various media, such as CO_2 at 700 °C for 24 h, H_2O at 100 °C for 24 h, and 30 ppm H_2S in Ar at 800 °C for 24 h. Approximately 1 g of the powder was placed in a clean alumina boat with a gas flow rate of ~25 cm^3/min. The reaction was allowed to run for 24 h, after which the furnace was cooled to room temperature; the gas flow was maintained during the heating and cooling cycles of the reaction. Then, the powdered samples were examined using PXRD. Scanning electron microscopy (SEM) (Philips XL30 SEM) was used to study the morphology of the as-prepared samples in the pellet form. SEM images of the Pt electrode surface, employed for electrical measurements, were obtained without a gold layer. A thin gold layer was sputtered for SEM measurements of the as-prepared compounds.

(11) Bhella, S. S.; Thangadurai, V. *J. Power Sources* **2009**, *186*, 311–319.
(12) Ryu, K. H.; Haile, S. M. *Solid State Ionics* **1999**, *125*, 355–367.
(13) Katahira, K.; Kohchi, Y.; Shimura, T.; Iwahara, H. *Solid State Ionics* **2000**, *138*, 91–98.
(14) Fabbri, E.; Epifanio, A. D.; Bartolomeo, E. D.; Licoccia, S.; Traversa, E. *Solid State Ionics* **2008**, *179*, 558–564.
(15) Fabbri, E.; Pergolesi, D.; Epifanio, A. D.; Bartolomeo, E. D.; Balestrino, G.; Licoccia, S.; Traversa, E. *Energy Environ. Sci.* **2008**, *1*, 355–359.
(16) Tao, S.; Irvine, J. T. S. *J. Solid State Chem.* **2007**, *180*, 3493–3503.
(17) Azad, A. K.; Irvine, J. T. S. *Solid State Ionics* **2008**, *179*, 678–682.
(18) Azad, A. K.; Savaniu, C.; Tao, S.; Dual, S.; Holtappels, P.; Ibberson, R. M.; Irvine, J. T. S. *J. Mater. Chem.* **2008**, *18*, 3414–3418.
(19) Nowick, A. S.; Du, Y. *Solid State Ionics* **1995**, *77*, 137–146.
(20) Bohn, H. G.; Schober, T.; Mono, T.; Schilling, W. *Solid State Ionics* **1999**, *117*, 219–228.
(21) Schober, T.; Bohn, H. G.; Mono, T.; Schilling, W. *Solid State Ionics* **1999**, *118*, 173–178.
(22) Valkenberg, S.; Bohn, H. G.; Schilling, W. *Solid State Ionics* **1997**, *97*, 511–515.
(23) Tao, S. W.; Irvine, J. T. S. *Adv. Mater.* **2006**, *18*, 1581–1584.

Table 1. Indexed PXRD Data for $AZn_{0.33+x}Nb_{0.67-x}O_{3-\delta}$ (A = Sr or Ba; x = 0 or 0.06)

			A = Sr; x = 0			A = Sr; x = 0.06			A = Ba; x = 0			A = Ba; x = 0.06		
h	k	l	d_{obs} (Å)	d_{calc} (Å)	I_{obs} (%)	d_{obs} (Å)	d_{calc} (Å)	I_{obs} (%)	d_{obs} (Å)	d_{calc} (Å)	I_{obs} (%)	d_{obs} (Å)	d_{calc} (Å)	I_{obs} (%)
1	0	0	4.015	4.003	2	3.994	3.993	3	4.085	4.091	4	4.081	4.090	6
1	1	0	2.831	2.830	100	2.820	2.824	100	2.890	2.893	100	2.890	2.892	100
1	1	1	2.311	2.311	4	2.304	2.305	8	2.360	2.362	12	2.360	2.362	9
2	0	0	2.001	2.001	37	1.997	1.997	43	2.045	2.045	30	2.045	2.045	21
2	1	0	1.786	1.786	1	1.783	1.786	1	1.829	1.830	3	1.829	1.829	2
2	1	1	1.634	1.634	41	1.631	1.786	59	1.670	1.670	45	1.670	1.670	30
2	2	0	1.416	1.415	19	1.413	1.412	27	1.447	1.446	20	1.446	1.446	11
3	0	0	–	–	–	–	–	–	1.364	1.364	19	1.364	1.363	2
3	1	0	1.266	1.266	14	1.265	1.263	10	1.294	1.294	2	1.294	1.294	15
			a = 4.003(3) Å			a = 3.993(1) Å			a = 4.090(6) Å			a = 4.090(5) Å		

Table 2. Values of X, Y, and Y_0 for $AZn_{0.33+x}Nb_{0.67-x}O_{3-\delta}$ (A = Sr or Ba; x = 0) and Selected Ordered and Disordered Perovskites

compound	X	Y	Y_0	expected structure	observed structure	refs
$SrZn_{0.33}Nb_{0.67}O_3$	1.63	−1.309	−0.797	disordered	disordered	this study
$BaZn_{0.33}Nb_{0.67}O_3$	1.63	−1.490	−0.797	disordered	disordered	this study
$SrMg_{0.33}Nb_{0.67}O_3$	1.62	0.513	−0.770	ordered	ordered	28
$BaMg_{0.33}Nb_{0.67}O_3$	1.62	0.331	−0.770	ordered	ordered	28, 32, 40−42
$SrNi_{0.33}Nb_{0.67}O_3$	1.59	0.223	−0.725	ordered	ordered	28
$BaNi_{0.33}Nb_{0.67}O_3$	1.59	0.041	−0.725	ordered	ordered/disordered	28, 42
$SrCa_{0.33}Nb_{0.67}O_3$	1.76	0.747	−1.044	ordered	ordered	28, 43
$BaCa_{0.33}Nb_{0.67}O_3$	1.76	0.564	−1.044	ordered	ordered	28, 37−39
$SrCo_{0.5}Nb_{0.5}O_3$	1.06	0.281	−1.110	disordered	disordered	25, 32
$BaCo_{0.5}Nb_{0.5}O_3$	1.06	−1.29	−1.110	disordered	disordered	25, 32

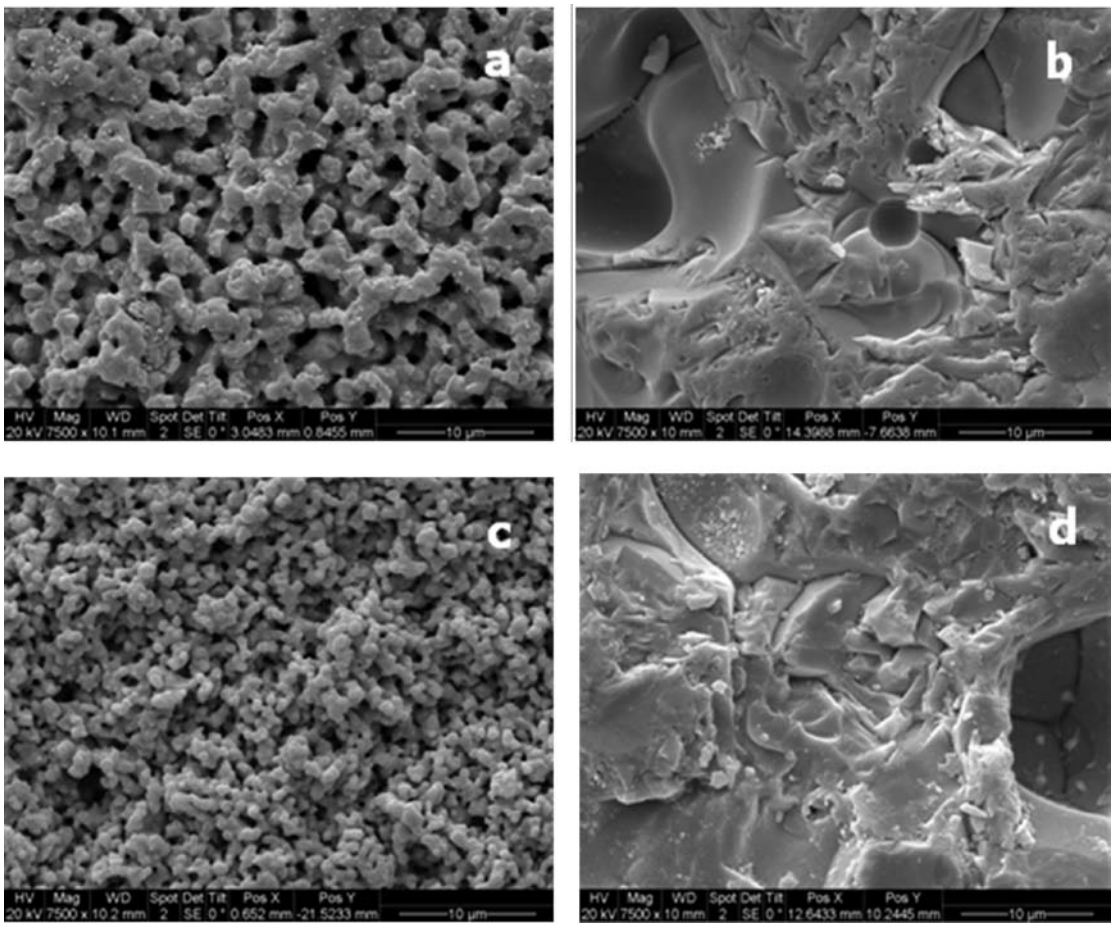

Figure 2. Typical SEM images of as-prepared (pellet) (a) $SrZn_{0.33}Nb_{0.67}O_3$, (b) $SrZn_{0.39}Nb_{0.61}O_{3-\delta}$, (c) $BaZn_{0.33}Nb_{0.67}O_3$, and (d) $BaZn_{0.39}Nb_{0.61}O_{3-\delta}$.

Electrical Characterization. The sintered pellets, which were cut into shorter width pellets (∼1.5−2 mm), were coated with Pt paste (LP A88-11S, Heraeus Inc.) on both sides of the pellet using a paint brush. The Pt-coated pellets were then dried at 900 °C for 1 h to remove the organic binders. Pt wires were attached to the surface of the pellet using a spring-loaded contact, which served as a current collector. Electrical conductivity measurements were performed in air, N_2 with 3% H_2O, N_2 with D_2O,

dry H_2, and H_2 with 3% H_2O using Pt as the electrode. The cell was heated at the desired temperature in the range of 300−800 °C using a Barnstead tubular furnace (model 21100) and held at a constant temperature for a minimum of 1 h and a maximum of 48 h prior to each measurement to allow the cell to equilibrate at the desired temperature and atmosphere. AC impedance (solartron electrochemical impedance spectroscopy; SI 1260, 100 mV; 0.01 Hz to 7 MHz) was used to determine the conductivity. A two-probe electrochemical cell was employed for the electrical characterization. The conductivity of each sample was measured by subsequent heating and cooling cycles. Also, different batch samples were used to ensure the reproducibility of the trend and magnitude of the values.

3. Results and Discussion

Phase Analysis. Figure 1 shows the PXRD patterns of $AZn_{0.33+x}Nb_{0.67-x}O_{3-\delta}$ (A = Sr or Ba). Both the Sr and Ba compounds can be indexed on a simple cubic (~4 Å) perovskite structure (Table 1 and Table S1 of the Supporting Information) in space group $Pm\bar{3}m$, in which both the Zn and Nb are randomly distributed at the B-site,[24] which is consistent with the model of Anderson et al.[25] However, the crystal structure of $AZn_{0.33}Nb_{0.67}O_3$ is known to exhibit several modifications, including disordered cubic and ordered hexagonal structures.[26−33] These allotropes are stabilized by different sintering temperatures. For example, Tolmer and Disgardin reported the formation of the hexagonal $BaZn_{0.33}Ta_{0.67}O_3$ at 1600 °C and a cubic phase at 1450 °C.[27] Glasso and Pyle also synthesized cubic $BaZn_{0.33}Ta_{0.67}O_3$ at 1400 °C in air.[28] Thirumal and Ganguli prepared cubic $Ba_{3-x}Sr_xZnNb_2O_9$ ($0 < x < 0.3$) by solid-state reaction at 1000−1200 °C.[29] Generally, a large difference in the ionic radius and charge of the B-site cations favors ordered perovskite structure over the random disordered cubic perovskite structure. Also, d^o cations such as Nb^{5+} and Ta^{5+} exhibit second-order Jahn−Teller distortions and are known to form out-of-center distorted octahedra in the perovskite-type structures.[30−33] Smaller A-site $SrNi_{0.33}Nb_{0.67}O_3$ crystallized in an ordered structure (hexagonal; a = 5.64 Å; c = 6.90 Å), while the corresponding Ba analogue was stabilized in a cubic (4.074 Å) structure.[28]

Formation of a simple cubic perovskite structure of the investigated compound may be explained by performing the well-known tolerance factor (t) calculation, as shown below:[33]

$$t = \frac{r_A + r_O}{\sqrt{2}(0.33r_B + 0.67r_{B'} + r_O)} \quad (1)$$

where r_A and r_O are the effective ionic radii of the A site ion and oxygen ion, respectively, and r_B and $r_{B'}$ represent the average effective ionic radii of the B and B′ site ions, respectively. Using Shannon's effective ionic radii,[34] the tolerance factors of $SrZn_{0.33}Nb_{0.67}O_3$ and $BaZn_{0.33}Nb_{0.67}O_3$

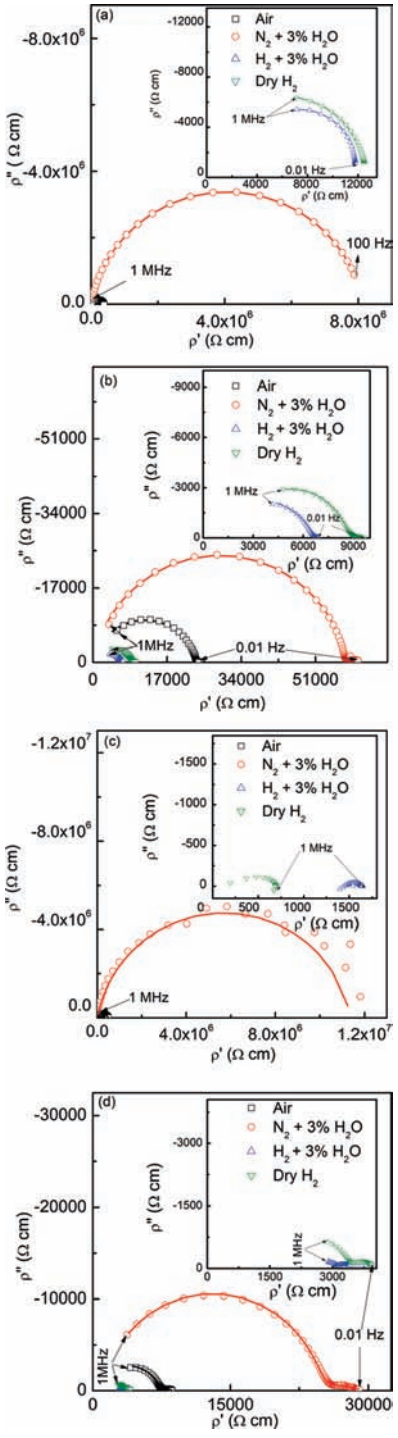

Figure 3. Typical AC impedance plots (converted into resistivity) for (a) $SrZn_{0.33}Nb_{0.67}O_3$ at 500 °C and (b) $SrZn_{0.39}Nb_{0.61}O_{3-\delta}$ at 700 °C in different atmospheres. (c and d) Corresponding Ba sample data. The insets show the data in an expanded view. The solid line passing through the data points represents the fitted data using the equivalent software. The absence of a tail in the low-frequency regime is clearly attributed to the reversible nature of the electrolyte−electrode interfaces. Unlike $BaCa_{0.39}Nb_{0.61}O_{3-\delta}$, the compounds investigated here show the absence of the grain boundary contribution to total electrical conductivity.

(24) (a) Anderson, M. T.; Vaughey, J. T.; Poeppelmeier, K. R. *Chem. Mater.* **1993**, *5*, 151–165. (b) Wong-Ng, W.; McMurdie, H. F.; Paretzkin, B.; Kuchinski, M. A.; Dragoo, A. L. *Powder Diffr.* **1988**, *3*, 179–187.
(25) Anderson, M. T.; Greenwood, K. B.; Taylor, G. A.; Poeppelmeier, K. R. *Prog. Solid State Chem.* **1993**, *22*, 197–233.
(26) Akbas, M.; Davies, P. K. *J. Am. Ceram. Soc.* **1998**, *81*, 1061–1064.
(27) Tolmer, V.; Desgardin, G. *J. Am. Ceram. Soc.* **1997**, *80*, 1981–1991.
(28) Galasso, F.; Pyle, J. *J. Phys. Chem.* **1963**, *67*, 1561–1562.
(29) Thirumal, M.; Ganguli, A. K. *Bull. Mater. Sci.* **2002**, *25*, 259–262.
(30) Lufaso, M. W.; Woodward, P. M. *Acta Crystallogr.* **2004**, *60*, 10–20.
(31) Anderson, M. T.; Poeppelmeier, K. R. *Chem. Mater.* **1991**, *3*, 476–482.
(32) Blasse, G. *J. Inorg. Nucl. Chem.* **1965**, *27*, 993–1003.
(33) (a) Bhuvanesh, N. S. P.; Gopalakrishnan *J. Chem. Mater.* **1997**, *6*, 2297–2306. (b) Lufaso, M. W.; Hopkins, E.; Bell, S. M.; Llobet, A. *Chem. Mater.* **2005**, *17*, 4250–4255. (c) Davies, P. K.; Wu, H.; Borisevich, A. Y.; Molodetsky, I. E.; Farber, L. *Annu. Rev. Mater. Res.* **2008**, *38*, 369–401.
(34) Shannon, R. D. *Acta Crystallogr.* **1976**, *32*, 751–767.

Table 3. AC Impedance Data for $AZn_{0.33+x}Nb_{0.67-x}O_{3-\delta}$ at 500 and 700 °C in Various Atmospheres

$AZn_{0.33+x}Nb_{0.67-x}O_{3-\delta}$	medium	T (°C)	R_b (Ω)	Q_b (pF)	n	C_b (pF)
A = Sr; x = 0	air	500	408.0k	130	0.84	19.9
		700	197.5k	31	0.90	8.0
	N_2 with 3% H_2O	500	8361.3k	27	0.89	9.6
		700	373.8k	133	0.80	11.2
	H_2	500	12.6k	50	0.90	10.2
		700	478	871	0.73	3.8
	H_2 with 3% H_2O	500	8839	21	0.99	17.5
		700	364	474	0.73	1.5
A = Sr; x = 0.06	air	500	1743.0k	33	0.94	17.7
		700	23.8k	133	0.87	20.0
	N_2 with 3% H_2O	500	1366.7k	32	0.95	22.0
		700	58.0k	84	0.89	18.5
	H_2	500	183.7k	143	0.86	25.6
		700	6114	96	0.93	32.6
	H_2 with 3% H_2O	500	98.0k	203	0.82	19.0
		700	6536	645	0.76	13.2
A = Ba; x = 0[a]	air	500	489.0k	135	0.81	14.1
		700	32.7k	78	0.88	13.5
	N_2 with 3% H_2O	500	11386.0k	61	0.89	24.8
		700	1003.8k	58	0.9	19.4
A = Ba; x = 0.06	air	500	339.5k	35	0.97	24.9
		700	7369	371	0.8	15.1
	N_2 with 3% H_2O	500	195.0k	108	0.89	28.7
		700	22.4k	63	0.94	26.8
	H_2	500	46.5k	252	0.83	24.6
		700	3467	1647	0.69	7.3
	H_2 with 3% H_2O	500	40.6k	748	0.8	55.5
		700	3080	7352	0.61	8.0

[a] Electrical fitting in H_2 atmospheres could not be estimated in the investigated frequency range.

are found to be 0.97 and 1.03, respectively, which lie in the range of the expected simple cubic perovskites.[33] Liu, Xuan, and Jia[35,36] have used the polarizability of the B site cations in the perovskites to predict the ordering of the structures. In this method, the empirical values of X, Y, and Y_0 for the desired perovskite ($ABB'O_3$) chemical formula can be calculated using the relationships[35,36]

$$X = \ln\left[\left|\frac{\text{charge}_B}{\text{ionic radius}_B} - \frac{\text{charge}_{B'}}{\text{ionic radius}_{B'}}\right|\right] \quad (2)$$

$$Y = \ln[(100|\text{difference in the polarizabilities of the B and B}' \text{ cations}|)/(\text{largest principal quantum number of the A atom} \times \text{number of total electrons in the outer electronic shells of the A atom})] \quad (3)$$

$$Y_0 = -1.9X + 2.3 \quad (4)$$

The magnitudes of X, Y, and Y_0 are used to understand the ordered and disordered arrangements of the B site cations (e.g., B = Zn, and B′ = Nb) in the structure. Authors have calculated these parameters for ~377 perovskite-type compounds in the $(A'A'')(B'B'')O_3$ system and have established a successful model for predicting the structure of the perovskites.[36] If the ln of the difference in the ratio of the charge to ionic radius (X), which is the ability of the B and B′ ions to polarize the nearby oxide ions, is greater than 1.8, then the corresponding compound should have an ordered structure. However, if the value is less than 1.8, then Y and Y_0 will determine the ordering of the structure. If Y is less than $Y_0 - 0.3$, then the compound is expected to form a disordered cubic perovskite, and if Y is greater than $Y_0 + 0.3$, then the compound is expected to form an ordered structure. We have performed these calculations on well-known B site ordered $BaCa_{0.33}Nb_{0.67}O_3$ and found that $X = 1.76$, $Y = 0.564$, and $Y_0 = -1.044$. Because $Y > Y_0 + 0.3$, BCN should be an ordered double perovskite structure and is consistent with the literature.[37−39] Table 2 lists the values of X, Y, and Y_0 for $AZn_{0.33}Nb_{0.67}O_{3-\delta}$ studied here together with those of a few selected ordered and disordered perovskites.[25,28,32,37−43] Figure 2 shows the typical SEM images of the investigated compounds. The particle to particle contact and the sizes of the particles were found to increase with increasing Zn content in both Sr and Ba compounds. The apparent density determined using the mass by volume ratio was found to support the investigated trend.

AC Impedance Spectroscopy. Figure 3 and Figure S2 of the Supporting Information show the typical AC impedance plots of $SrZn_{0.33}Nb_{0.67}O_3$ and $SrZn_{0.39}Nb_{0.61}O_{3-\delta}$ (Figure 3) and $BaZn_{0.33}Nb_{0.67}O_3$ and $BaZn_{0.39}Nb_{0.61}O_{3-\delta}$ (Figure S2), respectively, in various atmospheres at 500 and 700 °C. Similar patterns were observed for $SrZn_{0.35}Nb_{0.65}O_{3-\delta}$ and $SrZn_{0.41}Nb_{0.59}O_{3-\delta}$ and for $BaZn_{0.35}Nb_{0.65}O_{3-\delta}$ and $BaZn_{0.41}Nb_{0.59}O_{3-\delta}$. In all the

(35) Liu, R.; Xuan, Y.; Jia, Y. Q. *J. Solid State Chem.* **1997**, *134*, 420–422.
(36) Liu, R.; Xuan, Y.; Jia, Y. Q. *Mater. Chem. Phys.* **1998**, *57*, 81–85.
(37) Deng, J.; Chen, J.; Yu, R.; Liu, G.; Xing, X. *J. Alloys Compd.* **2009**, *472*, 502–506.
(38) Trejoa, E. R.; De Souzab, R. A. *J. Solid State Chem.* **2005**, *178*, 159–1967.
(39) Takahashi, T.; Wu, E. J.; van der Ven, A.; Ceder, G. *Jpn. J. Appl. Phys.* **2000**, *39*, 1241–1248.
(40) Yadong, D.; Guanghui, Z.; Liling, G.; Hanxing, L. *Solid State Commun.* **2009**, *149*, 791–794.
(41) Janaswamy, S.; Murthy, G. S.; Dias, E. D.; Murthy, V. R. K. *Mater. Lett.* **2002**, *55*, 414–419.
(42) Lufaso, M. W. *Chem. Mater.* **2004**, *16*, 2148–2156.
(43) Hevieu, M.; Raveau, B. *J. Solid State Chem.* **1979**, *28*, 209–222.

Table 4. Bulk Electrical Conductivities (σ) and Bulk Dielectric Constants (ε) of $AZn_{0.33+x}Nb_{0.67-x}O_{3-\delta}$ (A = Sr or Ba) at 500 and 700 °C in Air

compound	$\sigma_{500\ °C,air}$ (S cm^{-1})	$\sigma_{700\ °C,air}$ (S cm^{-1})	$\varepsilon_{500\ °C,air}$	$\varepsilon_{700\ °C,air}$
$SrZn_{0.33}Nb_{0.67}O_3$	5.1×10^{-7}	3.1×10^{-7}	45.4	18.9
$SrZn_{0.35}Nb_{0.65}O_{3-\delta}$	1.3×10^{-7}	6.1×10^{-6}	56.1	49.6
$SrZn_{0.39}Nb_{0.61}O_{3-\delta}$	1.7×10^{-7}	1.2×10^{-5}	59.8	68.5
$SrZn_{0.41}Nb_{0.59}O_{3-\delta}$	2.0×10^{-7}	1.5×10^{-5}	87.8	94.0
$BaZn_{0.33}Nb_{0.67}O_3$	4.0×10^{-7}	6.0×10^{-6}	35.9	25.1
$BaZn_{0.35}Nb_{0.65}O_{3-\delta}$	9.7×10^{-7}	4.1×10^{-5}	99.6	65.1
$BaZn_{0.39}Nb_{0.61}O_{3-\delta}$	5.6×10^{-7}	3.1×10^{-5}	81.2	50.2
$BaZn_{0.41}Nb_{0.59}O_{3-\delta}$	7.9×10^{-7}	3.0×10^{-5}	83.4	53.9

media and for all the x values in the Sr compound, only one semicircle is visible in the impedance plots. These impedance plots were resolved by fitting using one RC circuit, as shown in panels a and b of Figure 3, whereas for the Ba compound, two semicircles that were fitted using two RC circuits can be seen, as shown in panels c and d of Figure 3. However, the second semicircle is very small compared to other known Ba-based perovskites, such as BCN and BCY. As shown in Table 3, the capacitance values for the Sr compound were found to be on the order of 10^{-12} to 10^{-11} F, whereas for the Ba compound, the first semicircle gave a capacitance value ranging from 10^{-12} to 10^{-11} F and the second semicircle gave a capacitance value ranging from 10^{-6} to 10^{-4} F, which fall in the reported range of the bulk contribution and electrode−electrolyte interface contribution, respectively.[44,45] The absence of a tail at the low-frequency side indicates the nonblocking nature of the electrode−electrolyte interface. Figure 4 shows the typical Pt layer coating on the pellet surfaces, which shows the porous structure.

To further prove the absence of the grain boundary resistance and the use of a RC circuit for the Sr and Ba compounds in the high-frequency region, in Figure 5 and Figure S3 of the Supporting Information, we show the modulus versus frequency and imaginary impedance versus frequency plots.[45] Because of the clear presence of only one peak in the high-frequency region, it is evident that only one RC circuit may be required to fit the impedance data.[45] The actual capacitance could be calculated using the formula[46−48] $C = R^{(1-n)/n}Q^{1/n}$, where n is an empirical constant with a value between 0 and 1, Q is the pseudocapacitance, and R is the total resistance of the compound (Table 3). Using the capacitance calculated above, the dielectric constants (Table 4) of the SZN and BZN were calculated using the formula $\varepsilon = C/C_0$, where $C_0 = \varepsilon_0(A/d)$ ($\varepsilon_0 = 8.854 \times 10^{-12}$ F m^{-1}, A is the area of the pellet, and d is the thickness of the pellet).[49] The dielectric constant at 500 and 700 °C in air was found to increase with increasing Zn content in $AZn_{0.33+x}Nb_{0.67-x}O_{3-\delta}$. The bulk dielectric constant was found to be slightly higher than that of Thirmumal and Ganguli,[29] which may be as a result of a higher sintering temperature.

Figure 6 shows the AC impedance plots comparing N_2 and 3% H_2O with N_2 and D_2O at 600 °C for $SrZn_{0.33}Nb_{0.67}O_3$ and $BaZn_{0.33}Nb_{0.67}O_3$, which showed much higher conductivity in D_2O than H_2O, which is very unusual perovskite behavior compared to that of well-known fast proton-conducting BCN and BCY. A similar behavior may be anticipated for other members of the investigated perovskite group. This means that the substitution of Zn for Ca in BCN not only eliminated the grain boundary resistance, but also appeared to decrease proton conduction at elevated temperatures, resulting in mainly electronic conduction.[50] Figure 7 shows the electrical conductivity as a function of x in $AZn_{0.33+x}Nb_{0.67-x}O_{3-\delta}$. As

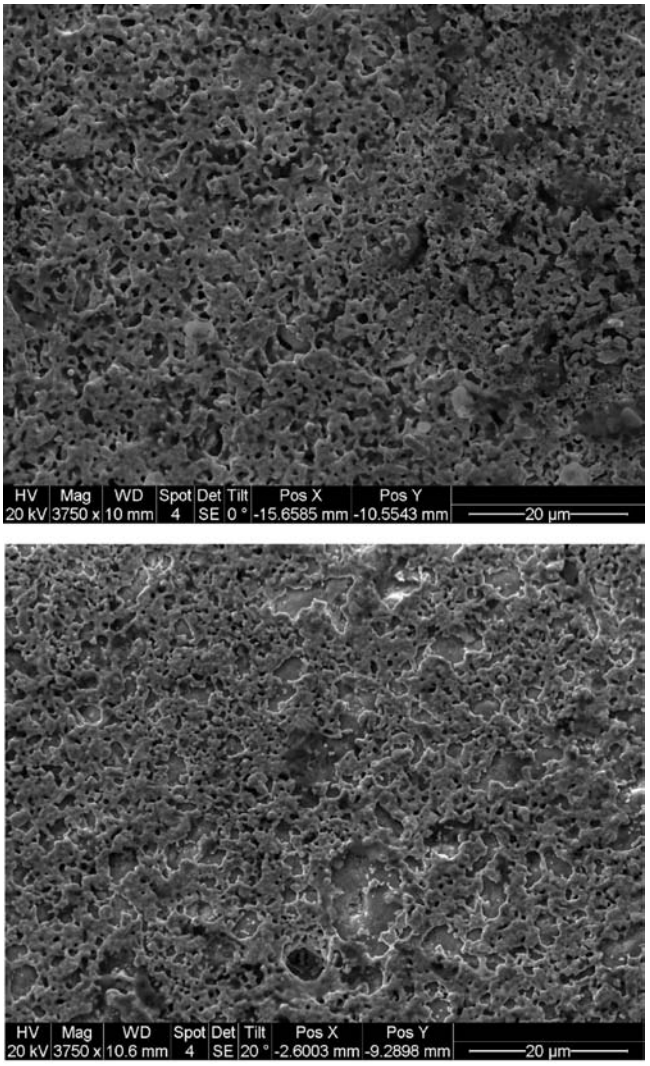

Figure 4. Comparison of the SEM images of Pt contacting $SrZn_{0.33}Nb_{0.67}O_3$ (top) and $BaZn_{0.33}Nb_{0.67}O_3$ (bottom) coated with platinum paste as the electrode.

(44) Baumann, F.; Fleig, J.; Habermeier, H. U.; Maier, J. *Solid State Ionics* **2006**, *177*, 1071–1081.
(45) Irvine, J. T. S.; Sinclair, D. C.; West, A. R. *Adv. Mater.* **1990**, *2*, 132–138.
(46) Li, Q.; Thangadurai, V. *Fuel Cells* **2009**, *9*, 684–698.
(47) Hjalmarsson, P.; Søgaard, M.; Mogensen, M. *Solid State Ionics* **2009**, *180*, 1395–1405.
(48) Chinarro, E.; Jurado, J. R.; Figueiredo, F. M.; Frade, J. R. *Solid State Ionics* **2003**, *160*, 161–168.
(49) Sagala, D.; Nambu, S. *J. Am. Ceram. Soc.* **1992**, *78*, 2573–2575.
(50) Bonanos, N. *Solid State Ionics* **2001**, *145*, 265–274.

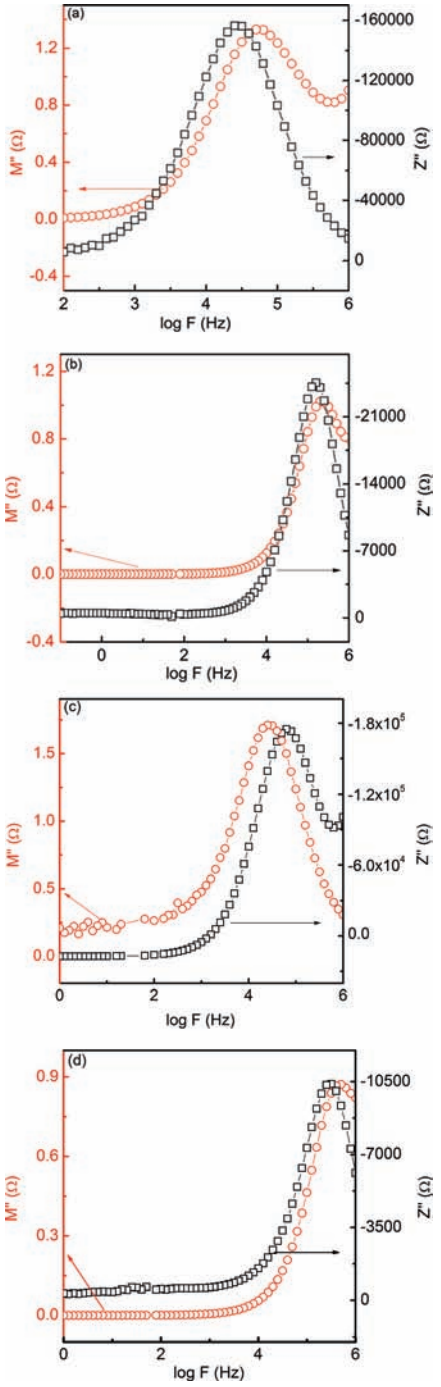

Figure 5. Typical modulus and Z'' as a function of frequency of (a) $SrZn_{0.33}Nb_{0.67}O_3$ at 500 °C in air, (b) $SrZn_{0.39}Nb_{0.61}O_{3-\delta}$ at 700 °C in wet N_2, (c) $BaZn_{0.33}Nb_{0.67}O_3$ at 500 °C in air, and (d) $BaZn_{0.39}Nb_{0.61}O_{3-\delta}$ at 700 °C in wet N_2. The presence of a single peak at a high frequency may correspond to a single contribution due to the electrical conductivity over the investigated frequency region.

the value of x increases, the conductivity seems to decrease in H_2; a similar trend was reported for $Sr_{4-x}M_xNb_2O_9$ (M = Cd, Cu, Ni, Zn) by Pantyukhina, Podkorytov, and Zhukovskii.[51] However, in air and wet N_2, an opposite trend was observed. As the Zn concentration increases, the conductivity seems to increase and

(51) Pantyukhina, M. I.; Podkorytov, A. L.; Zhukovskii, V. M. *Russ. J. Inorg. Chem.* **2010**, *55*, 103–111.

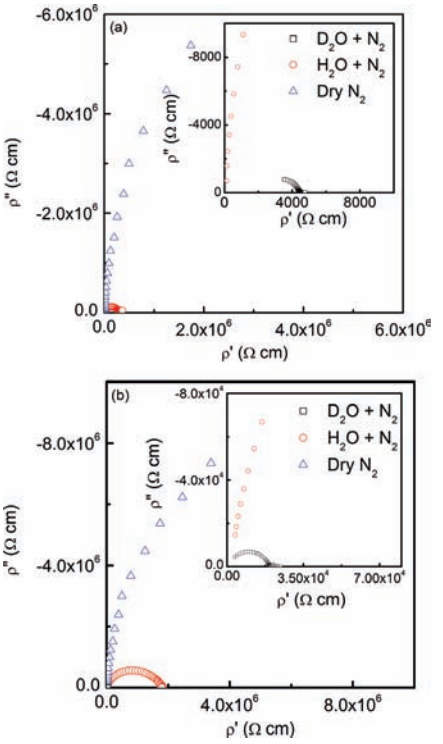

Figure 6. Typical AC impedance plots (converted into resistivity) for (a) $SrZn_{0.33}Nb_{0.67}O_3$ and (b) $BaZn_{0.33}Nb_{0.67}O_3$ in dry N_2, N_2 with 3% H_2O, and N_2 with D_2O at 600 °C.

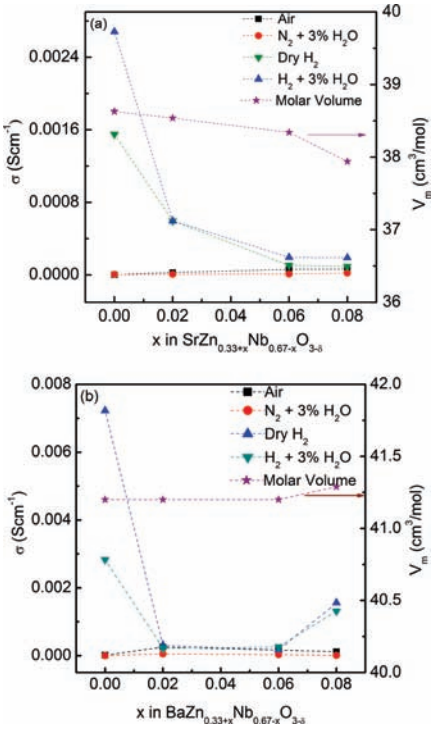

Figure 7. Variation of total electrical conductivity and molar volume as a function of x in (a) $SrZn_{0.33+x}Nb_{0.67-x}O_{3-\delta}$ and (b) $BaZn_{0.33+x}Nb_{0.67-x}O_{3-\delta}$ at 800 °C in various atmospheres. The electrical conductivity seems to decrease with increasing zinc content in dry and wet H_2.

could be ascribed to the formation of the oxide ion vacancies.

Figure 8 shows the Arrhenius plots for the $x = 0$ and $x = 0.06$ compounds for $AZn_{0.33+x}Nb_{0.67-x}O_{3-\delta}$ (A = Sr or

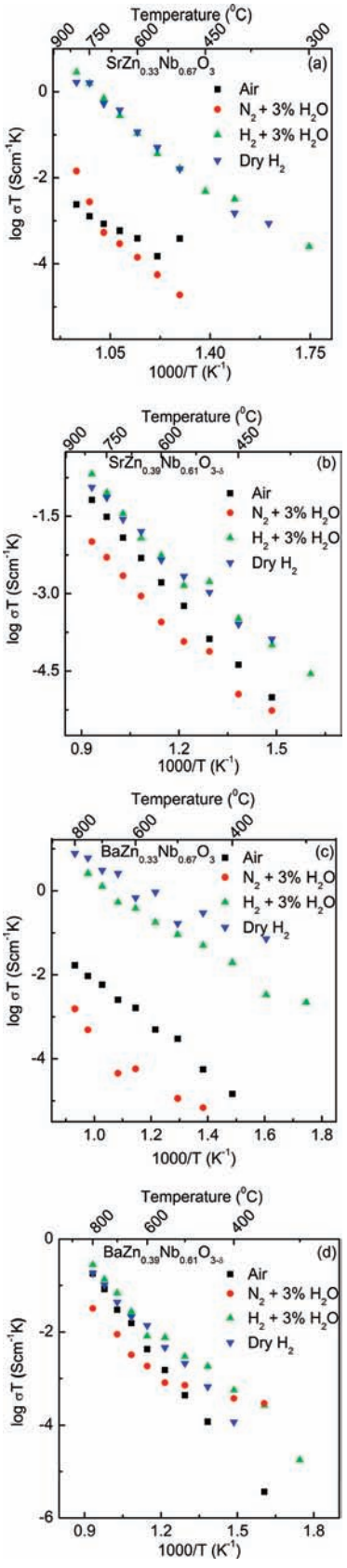

Figure 8. Arrhenius plots for total electrical conductivity of (a) $SrZn_{0.33}Nb_{0.67}O_3$, (b) $SrZn_{0.39}Nb_{0.61}O_{3-\delta}$, (c) $BaZn_{0.33}Nb_{0.67}O_3$, and (d) $BaZn_{0.39}Nb_{0.61}O_{3-\delta}$. The electrical conductivity was found to increase in H_2-containing atmospheres compared to that in air.

Ba and $x = 0.02$ and 0.08 members are shown in Figure S4 of the Supporting Information. The electrical conductivity

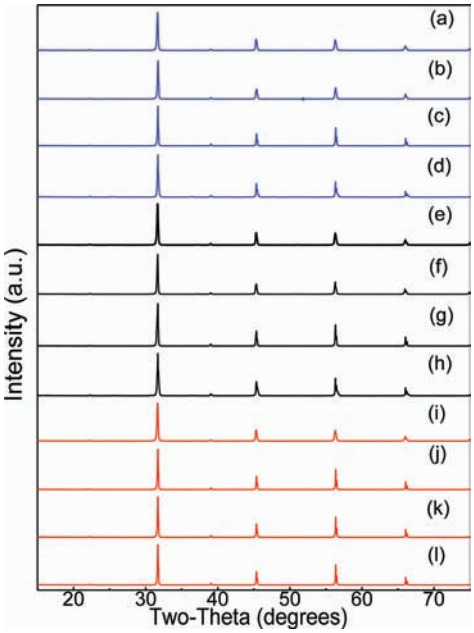

Figure 9. (a–d) PXRD of $x = 0$, 0.02, 0.06, and 0.08 compounds, respectively, of the formula $SrZn_{0.33+x}Nb_{0.67-x}O_{3-\delta}$, treated with CO_2 at 700 °C for 24 h. (e–h) Data for corresponding samples treated with H_2O at 100 °C for 24 h. (i–l) Data for corresponding samples treated with 30 ppm H_2S at 800 °C for 24 h.

data obtained during the heating and cooling cycles fall nearly on the same line, especially in air, suggesting that the equilibrium was reached. The conductivity achieved in wet H_2 for $SrZn_{0.33}Nb_{0.67}O_3$ was found to be more than 3 orders of magnitude higher than that in air, while for $BaZn_{0.33}Nb_{0.67}O_3$, conductivity in wet H_2 was ~2 orders of magnitude higher than that in air. The increase in electrical conductivity in H_2 could be mainly attributed to the electronic conduction due to the reduction of Nb because the electrical conductivity in D_2O showed an opposite trend versus that in H_2O. However, Zn content in $AZn_{0.33+x}Nb_{0.67-x}O_{3-\delta}$ seems to play an important role in the electrical conductivity in various atmospheres. For example, substituting Zn for Nb in $AZn_{0.33+x}Nb_{0.67-x}O_{3-\delta}$ seems to affect the order of increase in the electrical conductivity between air and H_2. This may not be attributed to potential leakage of the gases because the above trend appears to be valid for SZN and BZN members. Further work is required to understand the exact nature of the charge carriers in the investigated Zn-based perovskites as a function of oxygen, water, and hydrogen partial pressures over a wide range of temperatures. Among the studied compounds, the highest conductivity of 7.2×10^{-3} S cm^{-1} in dry H_2 at 800 °C was observed for $BaZn_{0.33}Nb_{0.67}O_3$.

Chemical Stability of $AZn_{0.33+x}Nb_{0.67-x}O_{3-\delta}$ (A = Sr or Ba). Figures 9 and 10 show the powder X-ray diffraction (PXRD) patterns produced by the CO_2 treatment at 700 °C for 24 h, the H_2O treatment at 100 °C for 24 h, and the 30 ppm H_2S treatment at 800 °C for 24 h for $x = 0$, 0.02, 0.06, and 0.08 in $AZn_{0.33+x}Nb_{0.67-x}O_{3-\delta}$ (A = Sr or Ba). Both $SrZn_{0.33}Nb_{0.67}O_3$ and $BaZn_{0.33}Nb_{0.67}O_3$ were found to be stable in CO_2- and H_2O-containing atmospheres for a long period of time because the diffraction patterns of the chemically treated samples are comparable to those of the as-prepared samples. $SrZn_{0.33}Nb_{0.67}O_3$ was also found to be stable to sulfur poisoning for a long period

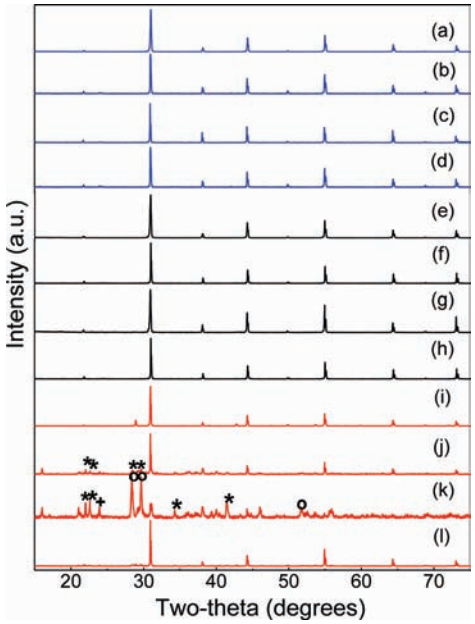

Figure 10. (a−d) PXRD of $x = 0$, 0.02, 0.06, and 0.08 compounds, respectively, of the formula $BaZn_{0.33+x}Nb_{0.67-x}O_{3-\delta}$, treated with CO_2 at 700 °C for 24 h. (e−h) Data for corresponding samples treated with H_2O at 100 °C for 24 h. (i−l) Data for corresponding samples treated with 30 ppm H_2S at 800 °C for 24 h. The perovskite-like structure was retained after the CO_2 and H_2O stability test, but was found to be unstable in 30 ppm H_2S. Peaks due to BaS (+) (JCPDS Card 01-0757), BaS_2 (O) (JCPDS Card 21-0087), and BaS_3 (∗) (JCPDS Card 03-0824) were observed at elevated temperatures.

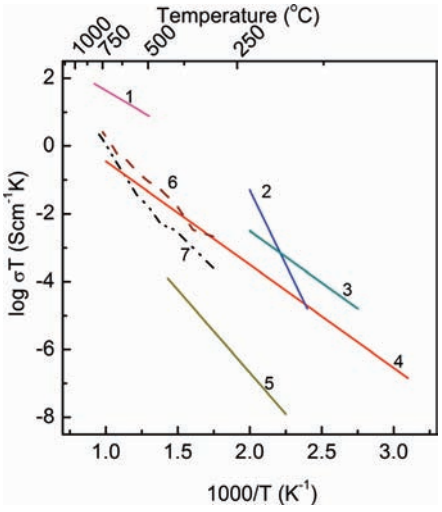

Figure 11. Comparison of the electrical conductivities of $AZn_{0.33}Nb_{0.67}O_3$ (A = Sr or Ba) in wet H_2 with those of other compounds.[22,52−56] (1) $BaCe_{0.9}Y_{0.1}O_3$ in a wet atmosphere. (2) $Sr_2Ga_{1.1}Nb_{0.9}O_{6-\delta}$ in H_2O/Ar medium. (3) $Sr_2Sc_{1.1}Nb_{0.9}O_{6-\delta}$ in a wet atmosphere. (4) $Ba_3Ca_{1.18}Nb_{1.82}O_{9-\delta}$ sintered at 1600 °C. (5) $Sr_2Nd_{1.05}Nb_{1.95}O_{6-\delta}$ in a wet atmosphere. (6) $BaZn_{0.33}Nb_{0.67}O_3$ (this work). (7) $SrZn_{0.33}Nb_{0.67}O_3$ (this work).

of time. However, $BaZn_{0.33}Nb_{0.67}O_3$ showed the formation of BaS (JCPDS Card 01-0757), BaS_2 (JCPDS Card 21-0087), and BaS_3 (JCPDS Card 03-0824) at 800 °C. In Figure 11, the total conductivities in wet H_2 of $SrZn_{0.33}Nb_{0.67}O_3$ and $BaZn_{0.33}Nb_{0.67}O_3$ are compared to those of other compounds in wet atmospheres.[22,52−56] $SrZn_{0.33}Nb_{0.67}O_3$ and $BaZn_{0.33}Nb_{0.67}O_3$ at 800 °C in wet H_2 have conductivities only ~1.5 orders of magnitude lower than that of the well-known $BaCe_{0.9}Y_{0.1}O_3$. However, unlike BCY, which is very unstable in CO_2-, H_2O-, and S-containing atmospheres,[14,56] $SrZn_{0.33+x}Nb_{0.67-x}O_{3-\delta}$ appears to be stable in all of these atmospheres for 24 h.

4. Conclusions

In summary, using the PXRD results, we can conclude that a single-phase perovskite with the $AZn_{0.33+x}Nb_{0.67-x}O_{3-\delta}$ formula (A = Sr or Ba; $0 \le x \le 0.08$) with disordered Zn and Nb at the B sites of space group $Pm\bar{3}m$ was prepared using the conventional solid-state reaction. Mainly bulk contribution to the total resistance with negligible grain boundary resistance was observed in the AC impedance investigations. Conductivity in the N_2/D_2O medium was found to be much better than that in the N_2/3% H_2O medium, which is significantly different from that of B site ordered perovskite $BaCa_{0.33+x}Nb_{0.67-x}O_{3-\delta}$ (BCN) and disordered doped $BaCeO_3$. The bulk dielectric constant was found in the range of 35−100 over the temperature range of 500−700 °C in air, which along with the electrical conductivity was found to increase with an increasing zinc concentration. However, an opposite trend was observed in dry H_2 and wet H_2 where the electrical conductivity decreased with increasing zinc content. The highest conductivity of 7.2×10^{-3} S cm^{-1} was achieved for $BaZn_{0.33}Nb_{0.67}O_3$ at 800 °C in dry H_2. Long-term structural and chemical stability in CO_2 at 700 °C and H_2O at 100 °C was achieved in Sr and Ba compounds. The Sr member with the $AZn_{0.33+x}Nb_{0.67-x}O_{3-\delta}$ formula was further proven to be stable when tested in 30 ppm H_2S at 800 °C for longer periods of time, while the Ba compound formed reaction products such as BaS (JCPDS Card 01-0757), BaS_2 (JCPDS Card 21-0087), and BaS_3 (JCPDS Card 03-0824) at 800 °C.

Acknowledgment. This research was supported by funding to the NSERC Solid Oxide Fuel Cell Canada Strategic Research Network from the Natural Science and Engineering Research Council (NSERC) and other sponsors listed at www.sofccanada.com. We also thank the NSERC for funding through the Research Tools and Instruments and Infrastructure grants (RTI) (cat. 1) and the Canada Foundation for Innovation (CFI) for their financial support. We also thank Dr. V. I. Birss (Department of Chemistry, University of Calgary) for useful discussions. We thank Dr. S. S. Bhella for his assistance with SEM and electrical measurements. We thank B. Mirfakhraei and W. H. Kan for their assistance with H_2S stability tests and X-ray measurements.

Supporting Information Available: Additional experimental data. This material is available free of charge via the Internet at http://pubs.acs.org.

(52) Oishi, M.; Akoshima, S.; Yashiro, K.; Sato, K.; Mizukaki, J.; Kawada, T. *Solid State Ionics* **2008**, *179*, 2240–2247.

(53) Liang, K. C.; Nowick, A. S. *Solid State Ionics* **1993**, *61*, 77–81.

(54) Nowick, A. S.; Du, Y.; Liang, K. C. *Solid State Ionics* **1999**, *125*, 303–311.

(55) Liang, K. C.; Du, Y.; Nowick, A. S. *Solid State Ionics* **1994**, *69*, 117–120.

(56) Hung, M.; Peng, H. W.; Zheng, S. L.; Lin, C. P.; Wu, J. S. *J. Power Sources* **2009**, *193*, 155–159.